^{1}H Two-Dimensional Nuclear Overhauser Effect and Relaxation Studies of Poly(dA)·Poly(dT)†

Ronald W. Behling and David R. Kearns*

Department of Chemistry, University of California at San Diego, La Jolla, California 92093

Received September 9, 1985; Revised Manuscript Received January 6, 1986

ABSTRACT: The structure of poly(dA)·poly(dT) in aqueous solution has been studied by using ^{1}H two-dimensional nuclear Overhauser effect (2D NOE) spectroscopy and relaxation rate measurements on the imino and nonexchangeable protons. The assignments of the ^{1}H resonances are determined from the observed cross-relaxation patterns in the 2D NOE experiments. The cross-peak intensities together with the measured relaxation rates show that the purine and pyrimidine strands in poly(dA)·poly(dT) are equivalent in aqueous solution. The results are consistent with a right-handed B-form helix where the sugars on both strands are in the C2′-endo/anti configuration. These observations are inconsistent with a proposed heteronomous structure for poly(dA)·poly(dT) [Arnott, S., Chandrasekaran, R., Hall, I. H., & Puigjaner, L. C. (1983) *Nucleic Acids Res. 11*, 4141–4155]. The measured relaxation rates also show that poly(dA)·poly(dT) has fast, large-amplitude local internal motions (±20–25°) in solution and that the amplitudes of the base and sugar motions are similar. The motion of the bases in poly(dA)·poly(dT) is also similar to that previously reported for poly(dA-dT)·poly(dA-dT) and poly(dG-dC)·poly(dG-dC) [Assa-Munt, N., Granot, J., Behling, R. W., & Kearns, D. R. (1984) *Biochemistry 23*, 944–955; Mirau, P. A., Behling, R. W., & Kearns, D. R. (1985) *Biochemistry 24*, 6200–6211].

Synthetic simple sequence DNAs have been widely used as models for DNA because they usually exhibit simpler spectra [NMR, circular dichroism (CD), IR, Raman] than natural DNA and provide experimental parameters used to model the results from natural DNA (Blooomfield et al., 1974). The simple sequence DNAs are also interesting because they are expected to exhibit extremes in their behavior (melting, conformation, stiffness). One simple sequence polymer that has been examined by several different techniques is poly(dA)·poly(dT). According to measurements of Hogan et al. (1983), the torsional stiffness of poly(dA)·poly(dT) is 20 times smaller than that of poly(dG)·poly(dC) but twice that of chicken erythrocyte DNA. The poly(dA)·poly(dT) sequence is especially interesting because of the recent evidence that short runs of $dA_{n=5,6}$ are curved and cause anomalous electrophoretic behavior in certain kinetoplast DNA (Simpson, 1979; Challberg & Englund, 1980; Hagerman, 1984; Wu & Crothers, 1984). Raman spectra show that above 5 °C the structure of poly(dA)·poly(dT) is of the B-genus DNA, although there are indications of repuckering (to C3′-endo furanose) at low temperatures (Thomas & Peticolas, 1983). Recent resonance Raman measurements suggest that the stacking of adening is similar in poly(dA)·poly(dT) and poly(rA), and from this it was concluded that the poly(dA) strand is probably of the A-type with a C3′-endo sugar ring pucker (Jolles et al., 1985). Also, the rate of exchange of the AH8 proton is intermediate between that expected for an A- or B-type helix (Benevides & Thomas, 1985), which is interpreted as consistent with a proposal of Arnott et al. (1983) that this molecule has a heteronomous structure where the purine chain has an A-helix geometry (C3′-endo/anti) and the pyrimidine chain has a B geometry (C2′-endo/anti).

In the present work, one-dimensional (1D) and two-dimensional (2D) NMR relaxation techniques are used to investigate the structure and molecular dynamics of poly(dA)·poly(dT). A main objective of this and previous studies (Kearns et al., 1981; Feigon et al., 1983; Assa-Munt et al., 1984; Behling & Kearns, 1985a; Mirau et al., 1985) has been to exploit the sensitivity of relaxation rate to interproton distances ($1/r^6$) to determine the structures of polynucleotides in solution. However, because the relaxation rates also depend on the overall and internal motions of the DNA, it has been necessary to evaluate the dynamic properties of this molecule as well. The results indicate that the high-frequency motions of the bases and backbone of poly(dA)·poly(dT) are similar to those found in other DNA [poly(dA-dT)·poly(dA-dT), poly(dG-dC)·poly(dG-dC) (Assa-Munt et al., 1984; Mirau et al., 1985)]. From analysis of the relaxation measurements, we have obtained a set of effective distances that serve to define many of the important structural features of this molecule. The two strands appear to have nearly identical conformations and close to B-form DNA. The results clearly show that the sugar pucker of both the A and T nucleosides are close to C2′-endo and not C3′-endo. Specific interproton distances found by NMR are compared with those predicted for different DNA geometries. A preliminary account of some of this work has been presented elsewhere (Behling & Kearns, 1985a,b,c).

Experimental Procedures

(*a*) *Sample Preparation.* Poly(dA)·poly(dT) was purchased from P-L Biochemicals (lot no. 675/79 and 709/41) and sonicated at 5–10 °C in 1 M NaCl, 10 mM ethylenediaminetetraacetic acid (EDTA), and 10 mM cacodylic acid at pH 7.0 for about 8 h with a Heat System-Ultrasonic W375 sonicator on 50% duty cycle. The sample was then centrifuged to remove metal particles eroded from the sonicator tip. The DNA was precipitated with ethanol, redissolved in a small amount of buffer (0.1 M NaCl, 1 mM EDTA, 10 mM cacodylate, pH 7.0), and recentrifuged to remove more metal particles. The poly(dA)·poly(dT) sample (~10 mL) was then

† This work was supported by the National Science Foundation (Grant PCM83-03374 to D.R.K.).

0006-2960/86/0425-3335$01.50/0

phenol extracted and dialyzed twice against 300 mL of 0.1 M NaCl, 10 mM EDTA, and 10 mM cacodylate, pH 7.0, to remove paramagnetic ions from the sample. The DNA was then ethanol precipitated and redissolved in 0.1 M NaCl and 10 mM phosphate buffer, pH 7.0, to a concentration of 20 mM in base pairs and placed in Wilmad 508 CP microcells for the NMR experiments. The DNA concentration was determined by measuring the OD_{260} and using ϵ = 13 200 mol of base pairs/L.

The average size of the poly(dA)·poly(dT) was determined to be 68 base pairs by running the DNA on a 7% polyacrylamide gel along with restriction fragments from an *Hae*III digest of pBR322 as size markers. From the staining pattern on the gel, it is estimated that 90% of the DNA is within ±20 base pairs of the average length.

(*b*) *NMR Methods.* All proton spectra and relaxation measurements were made at 360 MHz on a home-built spectrometer based on an Oxford Instruments magnet and a Nicolet 1180 computer with a 293A′ pulse programmer. Phase cycling was done both by the Nicolet software and by a hard-wired phase cycler designed by Dr. John M. Wright. The temperature of the sample was regulated by passing cooled or heated nitrogen through the probe.

The spin–spin relaxation rates (R_2) of the imino proton in H_2O solution were measured by using the 90°–τ–180°–τ–Acq Hahn spin-echo experiment (Hahn, 1950) with the 1–1 pulse sequence (Moore & Kime, 1983) used for the 90° excitations and the 1–3–3–1 pulse sequence (Hore, 1983) for the 180° excitations. The R_2 of the nonexchangeable protons in D_2O solution were measured with the Hahn spin-echo method using hard pulses for the 90° and 180° inversions.

The nonselective spin–lattice rates (R_1^{NS}) of the nonexchangeable protons in D_2O solution were measured by using the 180°–τ–90°–Acq inversion–recovery sequence with phase alternation of the 90° observation pulse (T1IRAP). The R_1^{NS} of the imino proton in H_2O solution was measured with the T1IRAP method with a 15-ms homospoil placed immediately after the 180° hard pulse and a 1–3–3–1 pulse used for the 90° observation pulse to suppress the water signal.

Semiselective spin–lattice relaxation measurements of the imino proton in H_2O solution were performed by using the T1IRAP method with a 1–1 pulse for the 180° excitation and either a 1–1 or 1–3–3–1 pulse sequence for the 90° observation pulse.

Selective spin–lattice relaxation rates (R_1^S) of the nonexchangeable protons in D_2O solution were measured by using the T1IRAP method with the 180° pulse being either a 6–8-ms "soft" pulse (Early et al., 1980b) or a DANTE pulse (Morris & Freeman, 1978) with a total excitation time of 6–8 ms. In both cases, the carrier was placed on the selected resonance. The 90° observation pulse was a hard pulse.

Biselective relaxation rates (R_1^{BI}) of various pairs of nonexchangeable protons in D_2O solution were measured with the T1IRAP method where the observation pulse was a hard pulse. The two desired resonances were exicted by one of two methods, depending on the separation between the resonances. If the frequency separation was greater than ~1300 Hz ($^1/_2$ the frequency range of the DNA protons), the DANTE sequence was used for the 180° excitation with the carrier placed on one proton resonance and the delay between the hard pulses of the DANTE sequence adjusted so that the next excitation peak was on the other proton resonance. If the frequency separation between the desired proton resonances is less than ~1300-Hz proton resonance separation, the DANTE method cannot be used because the multiple excitations produced will no longer excite only two protons. The biselective excitation was then achieved audiomodulating a soft pulse to produce excitation at $\pm\nu_{mod}$ from the carrier.

All relaxation rates were determined by fitting the time-dependent decay of the magnetization with a least-squares fit to the appropriate equation. Both the R_2 and R_1^{NS} relaxation rates were fit with a single exponential. The other spin–lattice relaxation rates (e.g., R_1^S and R_1^{BI}) were fit with a sum of two exponentials, and the reported rate is the slope of the recovery curve at zero time determined from the fit. To check that this method gave reasonable values for the rate constants, several of the measurements were also fit by a kinetics analysis (Assa-Munt et al., 1984). The rate constants determined by these two methods agreed within 5–10% with the exponential fit giving slightly smaller rate constants.

Two-dimensional nuclear Overhauser effect (NOE) spectra of the nonexchangeable protons in D_2O solution were obtained by using either the standard (90°–τ_1–90°–τ_{mix}–90°–Acq) sequence or the accordion method (Bodenhausen & Ernst, 1981) where τ_{mix} is a multiple of the evolution time τ_1. Both methods were phase cycled to give pure absorption spectra (States et al., 1982).

Theory

The magnetic dipolar relaxation of protons in DNA has been discussed elsewhere (Assa-Munt et al., 1984; Mirau et al., 1985) and will be briefly summarized here.

(*a*) *Spin–Lattice Relaxation—Magnetic Dipolar Contribution.* The differential equation that describes the relaxation of spin i due to magnetic dipolar interactions with other spins, s, can be written as (Abragam, 1978)

$$dm_i/dt = -\tfrac{2}{3}m_i\sum_{s\neq i}K[J_0(\omega_i - \omega_s)(1 - m_s/m_i) + 3J_1(\omega_i) + 6J_2(\omega_i + \omega_s)(1 + m_s/m_i)] = -\sum_{s\neq i}m_i\rho_{is} - \sum_{s\neq i}m_s\sigma_{is} \quad (1)$$

$$\rho_{is} = \tfrac{2}{3}K[J_0(\omega_i - \omega_s) + 3J_1(\omega_i) + 6J_2(\omega_i + \omega_s)]$$

$$\sigma_{is} = \tfrac{2}{3}K[-J_0(\omega_i - \omega_s) + 6J_2(\omega_i + \omega_s)]$$

$$K = \gamma_i^2\gamma_s^2\hbar^2S(S + 1)r^{-6}$$

where m_i is $(M_z^i - M_{zo}^i)/M_{zo}^i$, M_z^i is the magnetization of spin i at time t and M_{zo}^i is the magnetization of spin i at equilibrium. For the large DNA fragments (~70 base pairs), the $J_0(\omega_H - \omega_H)$ spectral density is much larger than the $J_1(\omega_i)$ or $J_2(\omega_i + \omega_s)$ spectral densities ($J_0 \gg J_1, J_2$), so zero-quantum transitions dominate the selective spin–lattice and spin–spin relaxation. Consequently, these relaxation rates in large DNA molecules are expected and found to be field-independent (Assa-Munt et al., 1984; Behling & Kearns, 1985a). For an isotropic rotor, $J_n(\omega) = \tau_c/5[1 + (\omega\tau_c)^2]^{-1}$. Note in eq 1 that the contribution of the J_0 and J_2 spectral densities depends on the ratio of the s-spin magnetization to the i-spin magnetization, m_s/m_i. Therefore, the observed decay curve depends strongly on the relative degree to which spin i and spin s are excited. Another consequence is that, because of spin diffusion, as spin i relaxes (m_i decreases) the magnetization at the s spins (m_s) increases. Therefore, the observed relaxation rate can change as a function of time, and nonexponential relaxation can be expected.

To interpret the results of a spin–lattice relaxation rate measurement, it is crucial to understand the effect of different excitations. In the selective measurement (R_1^S), spin i is selectively excited ($m_s \neq 0$, $m_s = 0$, $m_s/m_i = 0$) and will initially relax rapidly due to the J_0 term. However, because of spin diffusion, the relaxation will slow and become nonex-

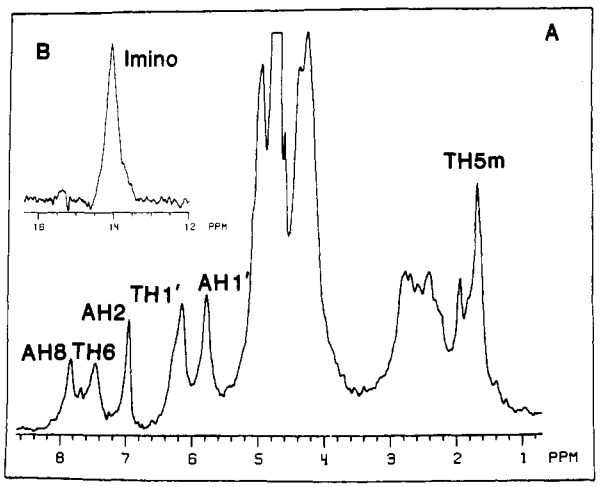

FIGURE 1: 360-MHz proton spectrum of poly(dA)·poly(dT) (A) nonexchangeable protons at 41 °C and (B) imino protons at 20 °C in 0.1 M NaCl and 10 mM phosphate buffer, pH 7.0.

ponential as m_s/m_i increases. In the nonselective measurement (R_1^{NS}), all spins are excited equally ($m_s/m_i = 1$) and the relaxation is much slower than R_1^S because only J_1 and J_2 terms remain (eq 1). A semiselective excitation strongly excites spin i and weakly excites the s spins so that $0 < m_s/m_i < 1$ so that $R_1^{NS} < R_1^{SEMI} < R_1^S$. In the biselective measurement (R_1^{BI}), spins i and s are equally excited, but the remaining spins are not excited. The difference $R_1^S - R_1^{BI}$ gives the cross-relaxation rate, σ_{is} (Broido & Kearns, 1982). The σ_{is} may be fast because it depends on the J_0 term and will also be field-independent.

(*b*) *Spin–Spin Relaxation—Magnetic Dipolar Contribution.* The spin–spin relaxation rate (R_2) between like ($\Delta\nu < R_2/\pi$) and unlike protons is given by (Abragam, 1978)

like spins

$$R_2^l = K[3J_0(0) + 5J_1(\omega_i) + 2J_2(2\omega_i)] \quad (2)$$

unlike spins

$$R_2^u = \tfrac{1}{3}K[4J_0(0) + J_0(\omega_i - \omega_s) + 3J_1(\omega_i) + 6J_1(\omega_s) + 6J_2(\omega_i + \omega_s)] \quad (3)$$

There are two important aspects of these equations. The first is that the R_2 of spin i does *not* depend on the magnetization of spin s (barring J-coupling effects) so a nonselective measurment may be used to measure R_2. The second point is that eq 3 shows that, in contrast to the R_1^S, R_2^u can be large even if $\omega_i - \omega_s$ is large because of the $J_0(0)$ term. This is the reason the ^{14}N–H interaction can make an important contribution to the R_2 of the imino protons even though the frequency difference between the interacting nuclei is large.

Another important result is that spin–spin relaxation between protons at the same resonance frequency, R_2^l, can be large. This is not the case for spin–lattice relaxation between like spins because both spins are always excited equally so that their contribution to the observed R_1 is just R_1^{NS}. Therefore, interactions with neighboring like protons (e.g., imino–imino) can contribute significantly to the observed R_2 yet have virtually no contribution to the observed R_1^S. In the slow motion limit, a proton interacting only with unlike protons will have an R_2/R_1^S ratio of 2.5. If there is a like interaction, this ratio will be larger than 2.5 (Behling & Kearns, 1985a).

Results

(*a*) *Two-Dimensional NOE of the Nonexchangeable Protons.* The 360-MHz proton spectrum of poly(dA)·poly(dT) at 41 °C is shown in Figure 1. Magnetic dipolar relaxation can result from a variety of interproton interactions, depending on the conformation of the DNA. To determine the important interactions in poly(dA)·poly(dT), 2D NOE spectra of the nonexchangeable protons were recorded. A 2D NOE contour plot of poly(dA)·poly(dT) at 41 °C in 0.1 M NaCl and 10 mM phosphate buffer, pH 7.0, obtained by using the accordion technique (Bodenhausen & Ernst, 1981) is shown in Figure 2. Cross sections through some of the peaks are shown in Figure 3. The cross-peaks in these spectra show which protons interact with one another and also provide a rough indication of the strength of the interaction between the protons. This interaction in turn provides an estimate of the internuclear distance, but note that the observed NOE also depends on the angle that the internuclear vector makes with the helix axis. The distance required to fit the observed interaction may vary up to 34%, depending on the angle that the internuclear vector makes with the helix axis. Examples of this can be seen in Figure 8.

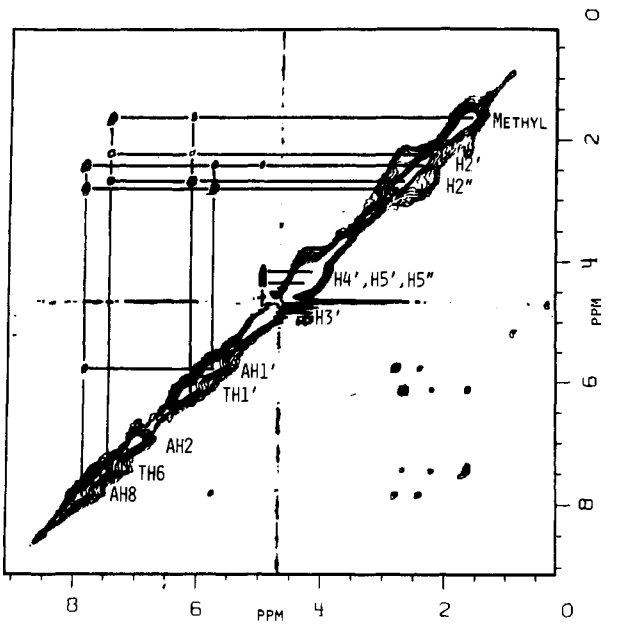

FIGURE 2: A 2D NOE spectrum of poly(dA)·poly(dT) at 41 °C in a D_2O solution of 0.1 M NaCl and 10 mM phosphate, pH 7.0. The spectrum was obtained by using a pure absorption accordion technique where the $\tau_{mix} = 8\tau_1$. Therefore, τ_{mix} ranged from 2.5 to 160 ms during the experiment.

The cross-peaks with the methyl proton resonances identify the TH6 (Figure 3A) and TH1′ (Figure 3B) resonances with the stronger cross-peak coming from the TH6. The AH2 resonance is identified by its weak cross-peak with both the AH1′ and TH1′ resonances. The TH1′–AH2 interaction is the only detectable cross-strand interaction in the molecule. The AH1′ resonance is identified by its strong cross-peak with the AH8 resonance (Figure 3B). The H2′ and H2″ resonances are identified by their cross-peaks with the H1′ resonances, and the H2″ is distinguished from the H2′ by its stronger cross-peak with the H1′ (Figure 3B). This observation of different intensities for the H1′–H2″ and H1′–H2″ cross-peaks shows that intensity distortions resulting from spin diffusion are not severe. The AH3′ and TH3′ resonances are identified by the strong cross-peaks with the H2′ and H2″ resonances. The H5′ assignment comes from its cross-peaks with the H1′, H2′, H2″, and H3′ resonances, although this assignment is much less certain than the other assignments. The AH4′, AH5″, TH4′, and TH5″ resonances must lie between 4.2–4.4 ppm to account for the observed intensity in the spectrum

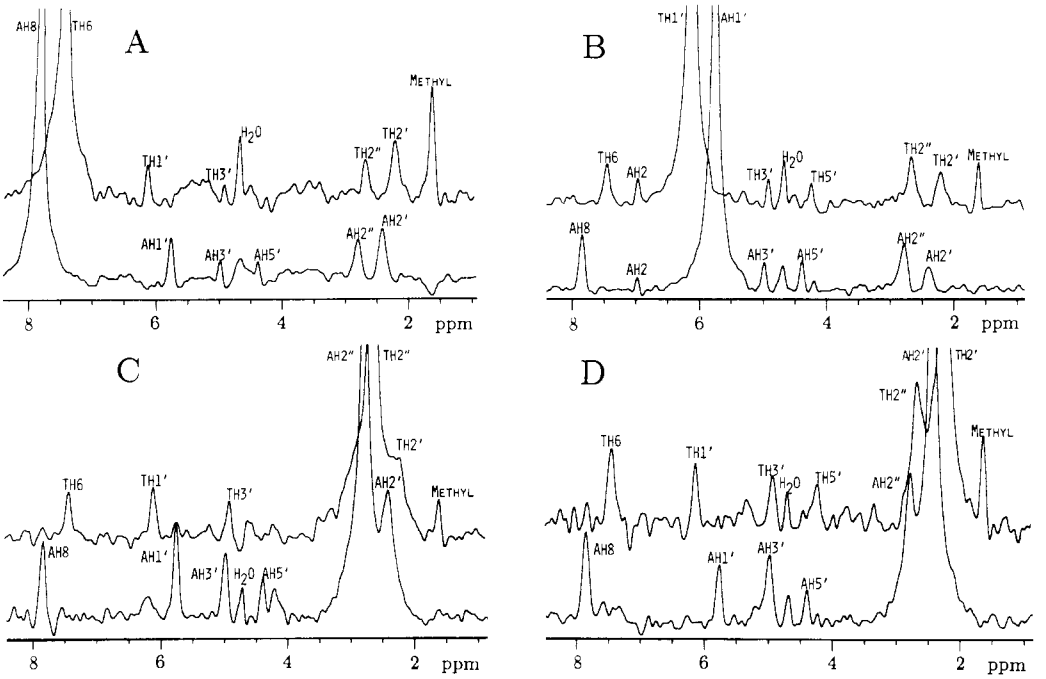

FIGURE 3: Cross sections of the 360-MHz 2D NOE accordion spectrum of poly(dA)·poly(dT) through (A) the AH8 and TH6 resonances, (B) the AH1′ and TH1′ resonances, (C) the AH2″ and TH2″ resonances, and (D) the AH2′ and TH2′ resonances. The peak assignments are as indicated. The DNA sample is in a D_2O solution of 0.1 M NaCl and 10 mM phosphate buffer, pH 7.0 at 41 °C.

Table I: Assignments and Chemical Shifts of Selected Protons in Poly(dA)·Poly(dT) at 41 °C in a D_2O Solution of 0.1 M NaCl and 10 mM Phosphate Buffer, pH 7.0[a]

proton	chemical shift (ppm)	proton	chemical shift (ppm)
AH8	7.9	AH4′	4.2
TH6	7.5	AH4′, AH5″, TH4′, TH5″	4.2–4.4
AH2	7.0	AH2″	2.8
TH1′	6.2	TH2″	2.7
AH1′	5.8	AH2′	2.4
AH3′	5.0	TH2′	2.2
TH3′	4.9	TH5m	1.6
TH5′	4.2		

[a] Chemical shifts are referenced to HOD at 4.66 ppm.

(Figure 1). A complete list of the proton resonance frequencies and assignments is given in Table I.

The cross sections also show that the interactions between protons on the A and T strands are of similar intensity, suggesting that both strands have similar conformations. In particular, the AH8 and TH6 have almost identical interactions with the H1′, H2′, and H2″ of their respective strands (Figure 3A,C). The observation that the AH8 and TH6 interact much more strongly with the H2′ and H2″ protons than the H3′ proton establishes that the sugars on both strands have C2′-endo rather than C3′-endo conformations. These results are inconsistent with a heteronomous model that C3′-endo conformation for the A strand in poly(dA)·poly(dT) (Arnott et al., 1983; Jolles et al., 1985).

(b) Magnetic Dipolar Relaxation of the Nonexchangeable Protons. A spin–spin relaxation rate (R_2) measurement on the nonexchangeable protons in poly(dA)·poly(dT) at 20 °C in a D_2O solution of 0.1 M NaCl and 10 mM phosphate buffer is shown in Figure 4A. A semilog plot recovery of one proton, the AH8, is shown in Figure 4B, and the spin–spin relaxation rates of selected protons are given in Table II.

An example of a selective relaxation rate (R_1^S) measurement on the AH8 is shown in Figure 4C,D. The recovery of the AH8 in a biselective spin–lattice relaxation rate (R_1^{BI}) measurement after simultaneous excitation of the AH8 and AH1′ protons is also shown in Figure 4D. The R_1^S and the cross-relaxation rates determined from $R_1^{Bi} - R_1^S$ for various protons, along with the nonselective spin–lattice relaxation rates (R_1^{NS}), are listed in Table II.

Table II: Magnetic Dipolar Relaxation Rates at 360 MHz of Selected Protons in Poly(dA)·Poly(dT) at 20 °C in 0.1 M NaCl and 10 mM Phosphate Buffer, pH 7.0

proton	R_1^S (s^{-1})	R_2 (s^{-1})	R_2/R_1^S	R_1^{NS} (s^{-1})	cross-relaxation rates (s^{-1})
AH8	38 ± 2	96 ± 5	2.5 ± 0.2	0.59 ± 0.03	σ(AH8–AH1′) = −10 ± 2
					σ(AH8–AH2′) = −15 ± 3
					σ(AH8–AH2′) = −13 ± 3
TH6	46 ± 3	115 ± 6	2.5 ± 0.2	0.53 ± 0.03	σ(TH6–TH1′) = −10 ± 5
					σ(TH6–TH2′) = −12 ± 4
					σ(TH6–TH2″) = −11 ± 4
					σ(TH6–TH5m) = −15 ± 4
AH2	2.8 ± 0.2	52 ± 2	19 ± 2	0.43 ± 0.02	R_2(AH2–AH2) = 45 ± 2
AH1′	39 ± 2	97 ± 4[a]	2.5 ± 0.2	0.54 ± 0.02	σ(AH1′–AH2″) = −14 ± 2
TH1′	38 ± 4	98 ± 3[a]	2.6 ± 0.3	0.55 ± 0.02	σ(TH1–TH2″) = −14 ± 4
					σ(TH1–TH5m) = −8 ± 4
TH5m	13 ± 1	56 ± 5	4.3 ± 0.5	0.72 ± 0.03	
imino	32 ± 7	148 ± 30	5.1 ± 0.7	0.4 ± 0.4	

[a] Inclusion of the effects of scalar coupling with the H2′ and H2″ protons could reduce the reported rate by 6%, assuming the maximum value of J = 15 Hz. The actual coupling constant depends on the sugar conformation.

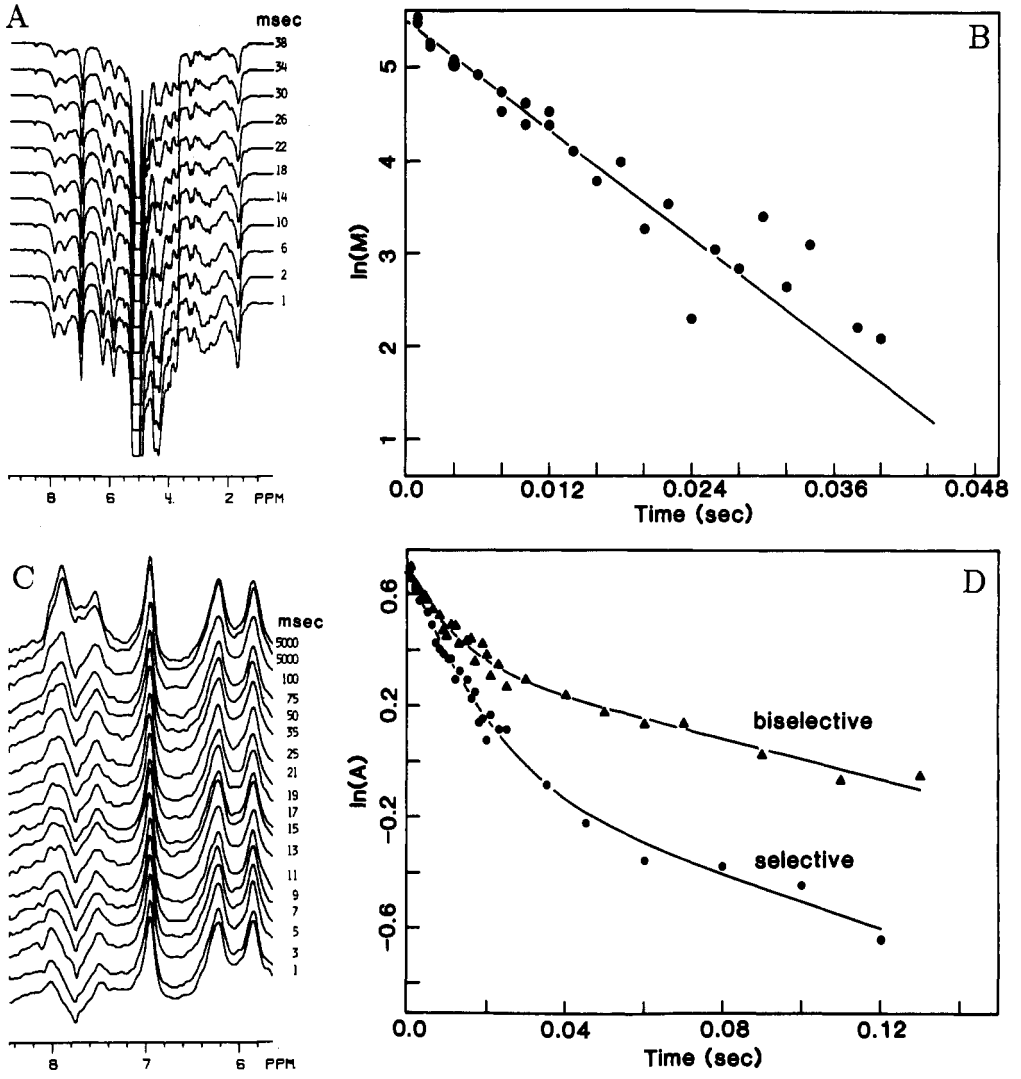

FIGURE 4: Spectra and recovery curves of relaxation experiments on the nonexchangeable protons of poly(dA)·poly(dT) at 20 °C in a D_2O solution of 0.1 M NaCl and 10 mM phosphate buffer at pH 7.0. (A) spin–spin relaxation rate (R_2) measurement. (B) Semilog plot of the spin–spin relaxation of the AH8. (C) A selective relaxation rate (R_1^S) measurement on the AH8 and TH6. Both protons may be excited simultaneously because cross-strand interactions are extremely weak. (D) Semilog plot of the selective relaxation of the AH8 and the relaxation of the AH8 after a biselective excitation of both the AH1′ and the AH8.

(*c*) *Magnetic Dipolar Relaxation of the Imino Proton.* An R_2 measurement on the imino proton at 20 °C in an H_2O solution of 0.1 M NaCl and 10 mM phosphate, pH 7.0, is shown in Figure 5A,B. The spin–lattice relaxation of the imino proton after a semiselective excitation is shown in Figure 5C,D. The imino proton relaxation rates are given in Table II. The nonexponential recovery magnetization after semiselective excitation illustrates the importance of spin diffusion in the spin–lattice relaxation and the sensitivity of the rates to the initial preparation of the spin system. The relaxation rate immediately following *selective* excitation of the imino proton depends only on J_0 (see Eq 1), but after some time there is an equilibration of the spin polarization among the four strongly interacting protons (two amino, imino, AH2). Relaxation then depends on the J_1 and J_2 terms (eq 1). Analysis of the experimental data to obtain values of specific rate constants is complicated because at long times transfer of magnetization from the 4 strongly interacting protons to the 19 nonexchangeable protons [spin diffusion, characterized by a rate constant R(exch–nonexch)] also contributes to the relaxation of the exchangeable protons (see Figure 6). If equilibration of magnetization with the 19-spin system occurs, the rate R_1^{NS}(nonexch) (rate at which the collection of 19 nonexchangeable protons relax after nonselective excitation when the exchangeable protons are absent) is also involved (Figure 6). To disentangle these various rate constants, we first directly evaluated R_1^{NS} (nonexch) by measuring the nonselective spin–lattice relaxation rate in 100% D_2O (see Table III for rates). Second, we evaluated the relaxation rate of the imino proton at long times after selective excitation, which gives R_1^{NS}(exch) + R(exch–nonexch) + R_{ex}*, where R_{ex}* is the exchange rate of the imino proton with solvent (R_{ex}) divided by the number of strongly interacting protons (4 in the case of A·T). R_{ex}* is important rather than R_{ex} because

Table III: Relaxation Rates Used To Determine R_1^{NS} of the Imino Proton in Poly(dA)·Poly(dT) at 20 °C[a]

relaxation measurement	rate (s^{-1})
nonexchangeable protons after nonselective excitation [R_1^{NS}(nonexch)] in D_2O	0.59 ± 0.08
imino proton exchange rate with solvent, R_{ex} (Mirau & Kearns, 1985)	2.5
imino proton at long times after selective excitation [R_{ex} + R(exch–nonexch) + R_1^{NS}(imino)][b]	4 ± 1
imino proton after exciting all DNA resonances in H_2O	0.63 ± 0.09
calcd imino R_1^{NS}	0.4 ± 0.4
calcd spin-diffusion rate connecting exchangeable and nonexchangeable protons [R(exch–nonexch)]	3.0 ± 0.4

[a] See Figure 6. [b] R_{ex}* = $R_{ex}/4$ = 0.6 s^{-1}.

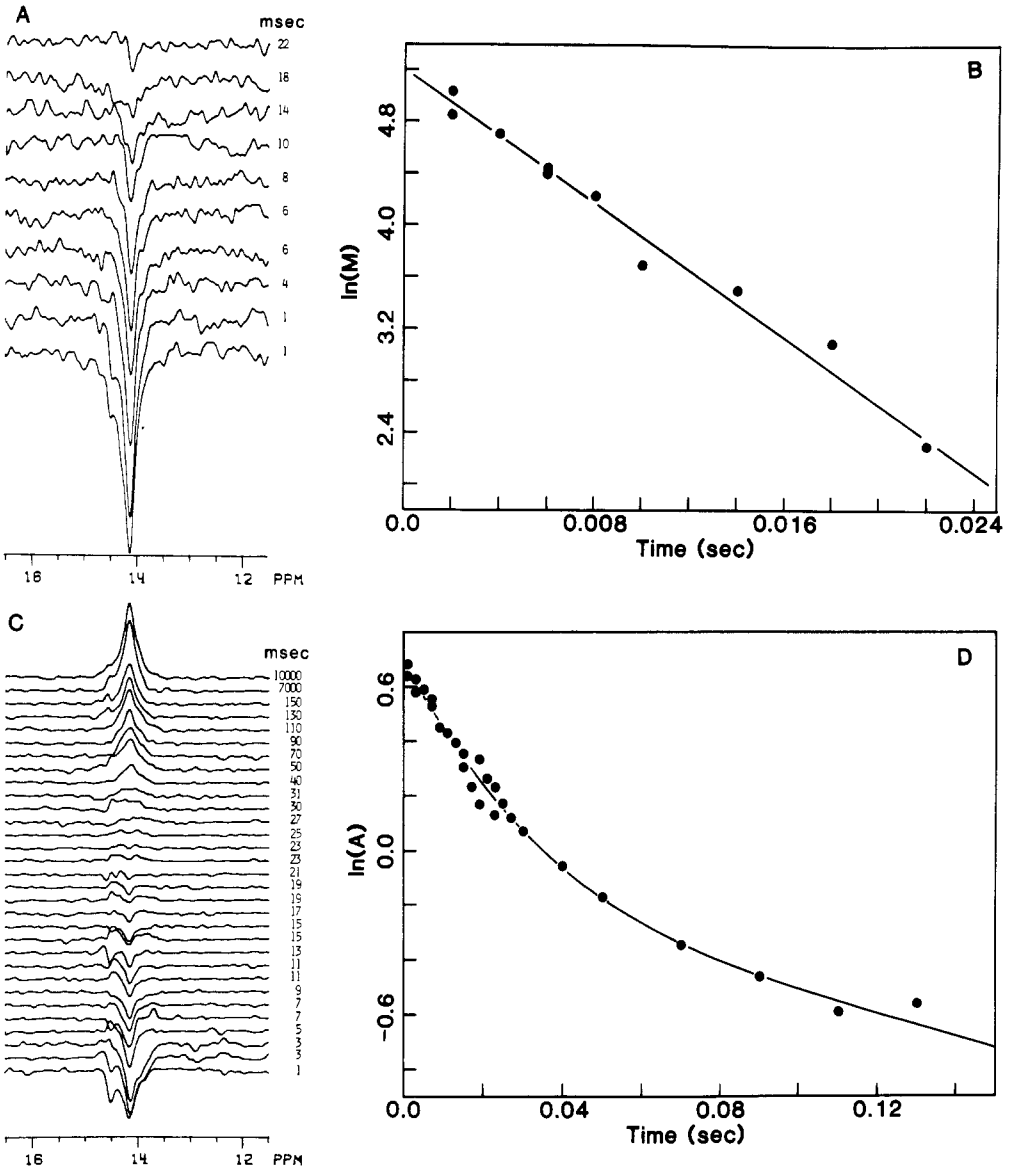

FIGURE 5: Spectra and recovery curves of relaxation measurements on the imino proton of poly(dA)·poly(dT) at 20 °C in an H_2O solution of 0.1 M NaCl and 10 mM phosphate buffer at pH 7.0. The glitch at ~14.2 ppm is from the carrier. (A, B) Spin–spin relaxation rate (R_2) measurement. (C, D) Relaxation of the imino proton after a semiselective excitation with the 1–3–3–1 pulse sequence.

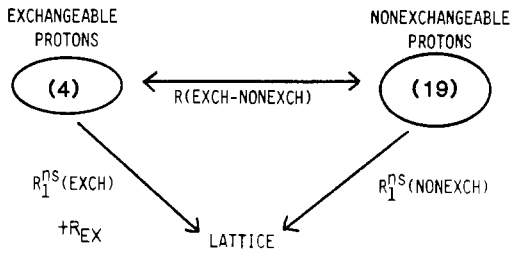

FIGURE 6: Schematic diagram representing relaxation pathways between the 19 strongly interacting nonexchangeable protons and the 4 strongly interacting base protons (two amino, imino, AH2) and the lattice. See text for explanation.

the new "cold" imino proton is rapidly polarized by the strong interactions with the neighboring nuclei. Third and last, we evaluated the relaxation rate of the imino proton following a nonselective excitation of *all* protons in the DNA molecule.

The values of R_1^{NS} (imino) and R(exch–nonexch) were obtained by fitting the imino proton relaxation curve resulting from nonselective excitation of all the DNA protons by using the kinetic model where the 4 strongly coupled protons (two amino, imino, AH2) interact with the 19 tightly coupled nonexchangeable protons (Figure 6). The value of R_1^{NS}(nonexch) is known, and we require that R_1^{NS} + R(exch–nonexch) + R_{ex}* for the imino proton be equal to the relaxation rate observed at long times after selective excitation of the imino proton. The effective exchange rate of the imino proton with solvent, R_{ex}*, is the exchange rate of the imino proton with solvent [R_{ez} = 2.5 s^{-1} (Mirau & Kearns, 1985)] divided by the number of strongly interacting spins, 4 in this case. Therefore, R_{ex}* is $1/4R_{ex}$* = 0.6 s^{-1}. The calculated values for R_1^{NS}(imino) and R(exch–nonexch) are given in Table III.

(*d*) *Analysis of Magnetic Dipolar Relaxation Rates.* A major difficulty in analyzing NMR relaxation rates and NOE's is that both depend strongly on internuclear distances and motions present in the system. If the internuclear geometry is known and the distances are fixed, then the observed relaxation rates (or NOE's) provide information about the motion, of the internuclear vectors. Conversely, accurate knowledge of the motional properties allows determination of structural information (distances, angles) from the NMR data if the distances are fixed or distance fluctuations occur on a much different time scale than the motions causing relaxation (e.g., vibrations of a C–H bond). Analysis of the NMR data

Table IV: Some of the Important Internuclear Distances for Use in Poly(dA)·Poly(dT) Imino Proton Calculations[a]

interaction	distance (Å)/angle to helix axis (deg)	interaction	distance (Å)/angle to helix axis (deg)
imino–AH61	2.41/93	imino–TN3	1.15/89
imino–AH62	3.90/99	imino–imino	3.46/12
imino–AH2	2.73/86		

[a] In the relaxation rate calculations, all interactions <6 Å were included. The interactions listed account for ~80% of the calculated R_1^S and ~90% of the calculated R_2 for B-DNA.

for DNA is further complicated because the motions that cause relaxation also alter the internuclear geometry. However, Keepers and James (1982) have performed theoretical calculations of the effect of fluctuations in the interproton separation on distance determinations and find that the effective distance obtained from relaxation measurements is approximately the arithmetic mean of the extremes of the motions, provided the excursions are small (e.g., 2.3 ± 0.3 Å). Therefore, we have assumed that interproton distances remain fixed at some effective distance even in the presence of motion and searched for geometries (combinations of interproton distance and orientation with respect to the helix axis) that fit the observed relaxation rates. In this way, effective internuclear geometries may be obtained.

The internal motion in the DNA molecule was evaluated from the relaxation of protons with fixed geometries. The "experimentally" determined spectral densities are then used to determine effective distances for nuclei where the internuclear distances may be sensitive to the exact DNA conformation.

In the A·T base pair, there are four interactions whose internuclear distances are independent of the DNA conformation: H1′–H2″, H5′–H5″, H2′–H2″, and TH6–TH5m (methyl protons). However, because of the overlap of resonances in the spectrum, only the TH6–TH5m interaction is useful. The length of this interaction is determined by calculating the value $\langle r^{-3}\rangle^{-1/3}$ of the distance from the TH6 to the path traced by the rotating methyl protons. The effective distance for each of the three TH6–TH5m interactions is 2.88 Å (Pegg et al., 1980).

The relaxation of the imino proton provides another monitor of the motion of the bases because the base pairing geometry is well established (Arnott & Hukins, 1972). Here, the geometry of the imino proton interactions is assumed fixed. The appropriateness of this assumption can be tested by comparing the mobility required to fit the TH6–TH5m data with the motions required to fit the imino proton data. The important interactions with the imino proton are listed in Table IV. These interactions contribute ~80% of the calculated R_1^S and ~90% of the calculated R_2. In the relaxation rate calculations, all interactions with distances less than 6 Å were included.

Given the assumption about the geometry of imino interactions, we have used several different models to fit the relaxation rates of the imino proton and the cross-relaxation rates for the TH6–TH5m interaction. While the internal motions of DNA are undoubtedly complex, Lipari and Szabo (1982) have shown that simplified motional models give reasonable estimates of amplitudes and frequencies of internal motion. Here, we attempt to fit the observed relaxation rates using models with the minimum of motion and the fewest possible parameters and increase complexity of the model to determine those features necessary to fit the observed relaxation rates. The results of the calculations are shown in Table V.

Model 1. The first and simplest model treats the DNA as a 68 base pair rigid rod in solution with correlation times described by the equations of Tirado and Garcia de la Torre (1980; Elias & Eden, 1981). This model reasonably accounts for the overall tumbling of the poly(dA)·poly(dT), since the persistence length is ~150 base pairs (Hogan et al., 1983), but does not allow any internal motion. In the rigid rod model, the DNA relaxation rates depend only on the tumbling times of the DNA helix about the long and short helix axes and the orientation of the internuclear vector about the long axis of the helix (Woessner et al., 1969). The rise per base pair is assumed to be 3.4 Å and the helix radius 13 Å. The viscosity of the DNA solution at 20 °C was assumed to be 1.0 cP. This model proves to be inadequate because the calculated values of R_1^S and R_2 are ~2 times larger than the observed values while the calculated R_1^{NS} is ~7 times too small.

Model 2. The second model incorporates the effect of collective torsional motions seen in fluorescence polarization anisotropy measurements (Genest & Wahl, 1978; Millar et al., 1981, 1982) by reducing the axial spinning time of the DNA from that calculated for a rigid rod to a shorter effective value. The torsional motions studied by the fluorescence polarization anisotropy of intercalated dyes in this laboratory (Hard & Kearns, 1986) suggest that poly(dA)·poly(dT) has an efffective correlation time of 6 ns for the axial rotation (τ_a). Although using this τ_a increases the calculated $R1^{NS}$, the calculated R_1^S and R_2 are still much too large.

Model 3. In the third model, helix bending or local motions along the helix axis are simulated by simply reducing the "effective" length of the DNA from 68 to 53 bp as in previous studies (Early & Kearns, 1979; Early et al., 1980a; Mirau et al., 1985). This decrease in length reduces the end-over-end tumbling correlation time (329 to 180 ns) and reduces rates that depend on J_0 (R_1^S and R_2). Comparison of these results with the results of the previous model shows that R_1^S and R_2 are much more sensitive to motions along the helix than to torsional motions.

Table V: Comparison of Imino and TH6–TH5m Relaxation Rates for Poly(dA)·Poly(dT) at 20 °C with Values Calculated by Using Various Motional Models[a]

	calcd rates (s^{-1})			
	imino			
	R_1^S	R_1^{NS}	R_2	σ(TH6–TH5m)
obsd values	32 ± 7	0.4 ± 0.4[a]	148 ± 30	−15 ● 4
model 1, 68-bp rigid rod, τ_l = 329 ns, τ_a = 18 ns	54	0.06	302	−30
model 2, 68-bp rod with "torsion", τ_l = 329 ns, τ_a = 6 ns	46	0.18	271	−26
model 3, 53-bp rigid rod, τ_l = 180 ns, τ_a = 14 ns	32	0.08	176	−18
model, 4, 68-bp rod with three-site jump, τ_l = 329 ns, τ_a = 18 ns, $\Delta\theta$ = 24°, τ_i = 3.2 ns	31	0.4	175	−17
model 5, 68-bp rod with "torsion" and three-site jump, τ_l = 329 ns, τ_a = 6 ns, $\Delta\theta$ = 20°, τ_i = 3.2 ns	29	0.44	173	−16
model 6, 68-bp rod with "torsion" and longitudinal and azimuthal jumps, τ_l = 329 ns, τ_a = 6 ns, τ_{lng} = 10 ns, $\Delta\theta$ = 22°, τ_{az} = 1 ns, $\Delta\phi$ = 20°	28	0.41	173	−14

[a] See text and Table III for an explanation of how this value was determined.

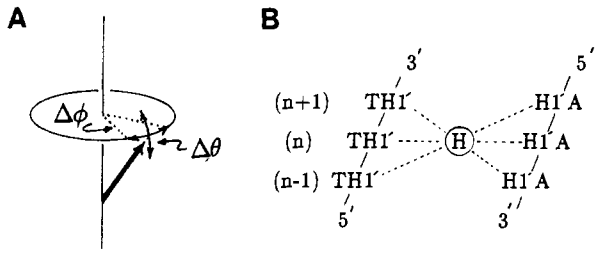

FIGURE 7: (A) Schematic diagram illustrating the azimuthal ($\Delta\phi$) and longitudinal ($\Delta\theta$) motions of an interproton vector relative to the DNA helix axis. (B) Schematic diagram showing the interactions of an AH2 proton with the H1′ sugar protons of neighboring bases.

Model 4. The fourth model is a rod with tumbling correlation times appropriate for a 68-bp rod in solution with internal motions simulated by a three-state jump on the surface of a cone (Woessner et al., 1969). Agreement with the observed data is achieved when the amplitude of jumping is ±24° with a correlation time of 3 ns.

Model 5. The fifth model includes the same internal motion as model 4, but the effect of collective torsional motion is included by setting the axial spinning rate to 6 ns. In this model, the amplitude of the jump is slightly reduced, but the correlation time for the internal motion remains unchanged at 3 ns.

Model 6. In the two previous models, the internal motion was simulated by jumps of the internuclear vector between sites on the surface of a cone that are 120° apart. The jumps therefore reorient the internuclear vector in both the longitudinal and azimuthal directions with the same rate. In the sixth model, the local longitudinal and azimuthal motions are decoupled and modeled as independent jumps with correlation times (jump rate = $1/2\tau$) τ_{lng} and τ_{az} and amplitudes $\Delta\theta$ and $\Delta\phi$, respectively (Wittebort & Szabo, 1978). A schematic diagram of the motion is given in Figure 7A. Collective torsional motions are included by setting axial spinning times to 6 ns. To fit the data, the longitudinal jump amplitude must be at least ±18° and generally in the 20–30° range for τ_{lng} <100 ns. The best fit of the data occurs with a longitudinal jump of ±22° with τ_{lng} = 10 ns and an azimuthal jump amplitude of ±15–25° with τ_{az} = 0.2–2.0 ns.

(e) Motion of the Sugar Rings in Poly(dA)·Poly(dT). The only fixed distances among the sugar protons are the H2′–H2″ and H5′–H5″ interactions, but because of overlapped resonance frequencies these protons cannot be studied by NMR in this molecule. All remaining proton–proton interactions among the nonexchangeable protons depend strongly on the sugar conformation, so their relaxation behavior cannot be used to rigorously determine the motion of sugar protons in poly(dA)·poly(dT). However, it is clear from the measurements of R_1^S, R_1^{NS}, and R_2 that the relaxation of the sugar protons has the same relaxation characteristics as other DNA systems. From frequency-dependent relaxation studies on 12 and 43 base pair restriction fragments (unpublished results), it has been determined that the sugar protons undergo motions with amplitudes of ±20–25° in the 0.5–1.0-ns time regime. These results are consistent with numerous other relaxation studies on sugar motions (Bolton & James, 1979; Early & Kearns, 1979; Hogan & Jardetzky, 1980; Levy et al., 1981, 1983; Keepers & James, 1982). We, therefore, will use these motional amplitudes for the sugar motions in poly(dA)·poly(dT).

(f) Comparison of NMR Results with Models Derived from X-ray Data. As stated previously, the observed relaxation rates depend on both internuclear distances and the motions present in the system. Since we have characterized the motions present in poly(dA)·poly(dT) (hence the spectral density terms in eq 1), the effective distance between any two protons can be determined if the relaxation rate arising from that interaction is known and the distance is assumed to be unaffected by the motions present. The strength of each pairwise interaction is given by the cross-relaxation rate, σ, between the two protons. Although it is difficult to quantify σ by NOE techniques in large DNA molecules because of spin diffusion,[1] the cross-relaxation rate can be determined by taking the difference between R_1^S and R_1^{BI} (Broido & Kearns, 1982). The cross-relaxation rates depend on the internuclear distances and the angles that the interaction vectors make with the helix axis as well as the motional properties.

The values of σ for selected pairs of protons are given in Table II. Plots of the allowed combinations of internuclear distance vs. angle of the interaction vector to the helix axis for eight of the interactions are shown in Figure 8. The allowed values fall between the curved lines on the plots. These plots were generated by choosing a value for the internuclear distance and calculating σ for each angle of the internuclear vector relative to the helix axis. This process was repeated for each internuclear distance in the range given on the plots. Contour lines were then drawn to show those combinations of internuclear distance and angle relative to the helix that give calculated σ's that fit the observed σ. Note that although the errors in the observed σ's are sometimes large, the errors in allowed distances determined by NMR are relatively small because of the $1/r^6$ dependence of the rate on the internuclear distance.

On these same plots are symbols representing the internuclear distance and orientation relative to the helix axis taken from three models based on X-ray diffraction studies on DNA fibers (Arnott & Selsing, 1974; Arnott et al., 1983; Arnott, personal communication). Protons were added where necessary to the heavy atom coordinates by using standard bond lengths and angles. None of the proposed models based on X-ray data fits the required structure determined by NMR, but the B and B′ forms are both reasonably close, with the B form providing the closest fit. Th heteronomous model of poly(dA)·poly(dT) fits the NMR results poorly.

DISCUSSION

The internal dynamics of poly(dA)·poly(dT) were examined by using proton relaxation rates. The major relaxation pathways of the nonexchangeable protons have been determined by 2D NOE measurments, and cross-relaxation rates for many interproton interactions have been measured. The DNA structure implied by the NMR results is then compared with the structures determined from X-ray diffraction studies on DNA fibers by Arnott and co-workers (Arnott & Selsing, 1974; Arnott et al., 1983; Arnott, personal communication).

[1] Recently Sarma et al. (1985) used presaturation NOE measurements on a heterogeneous (200 ± 50 bp) sample of poly(dA)·poly(dT) in an attempt to deduce its solution-state conformation. Although different presaturation pulse lengths and power were used, the shortest pulse was 20 ms, and their results are obviously complicated by extensive spin diffusion since the difference spectra are virtually identical at 20- and 50-ms irradiation times and the H3′, H2′, and H2″ have the same relative intensity at all irradiation times. This result is expected because the selective spin–latttice relaxation rates for most of the protons are between 30 and 50 s^{-1} for 70 bp long poly(dA)·poly(dT) and much faster spin-diffusion rates are expected in the longer DNA studied by Sarma et al. (1985). Consequently, short (few millisecond) irradiation pulses must be used if *primary* NOE's are to be measured without being overwhelmed by spin diffusion among many different protons. Because of these limitations, NOE's observed after 20 ms of presaturation of 200-bp poly(dA)·poly(dT) cannot be used to draw conclusions regarding structure.

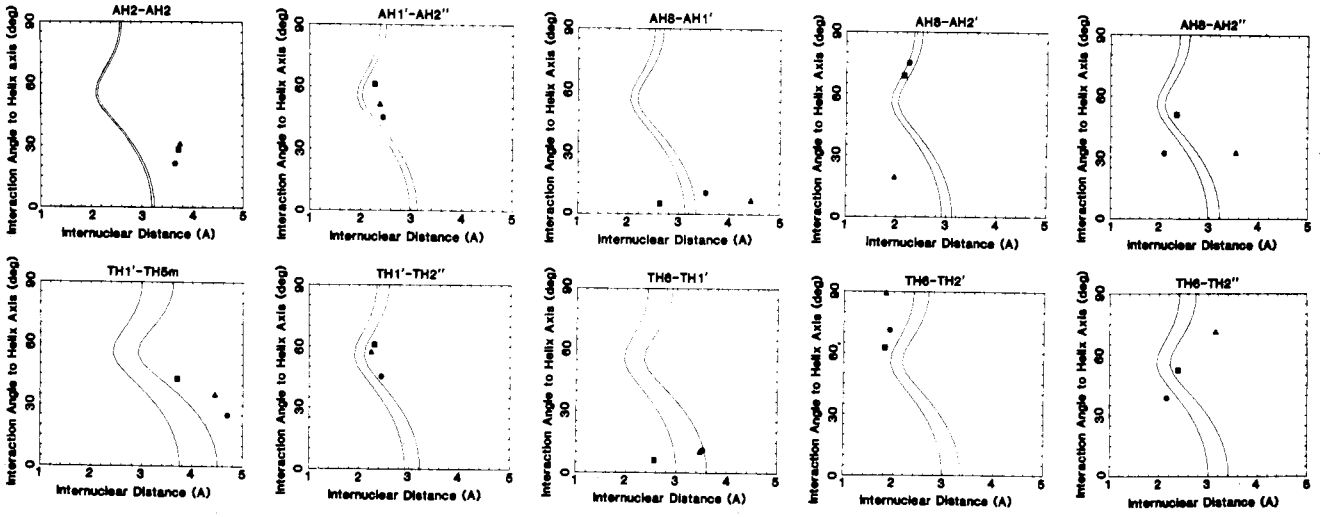

FIGURE 8: Contour plots showing the allowed combinations of internuclear distances and angles to the helix for several interproton interactions in the poly(dA)·poly(dT) molecule. The interacting protons are indicated at the top of the plot. The allowed geometries, which fall between the two contour lines on the plot, fit the cross-relaxation rate σ between the two interacting protons except for the AH2–AH2 interaction, where the interaction strength is determined from the R_2/R_1^S ratio. The plots also show interaction geometries predicted by models derived from X-ray data on DNA fibers. The models are a B-form DNA (●) (Arnott, personal communication), a B′ structure (■) (Arnott & Selsing, 1974), and the heteronomous structure for poly(dA)·poly(dT) (▲) (Arnott et al., 1983). These symbols show the distance and angle to the helix axis for the proton interaction except for the TH1′–TH5m interaction, where the symbols show the TH1′–TC5m geometry.

(*a*) *Internal Motion in Poly(dA)·Poly(dT).* The measured proton relaxation rates provide information about the fluctuations in DNA structure that occur in the nanosecond time range. By comparing the rates calculated by using different models for the DNA motions, we are able to identify the types of motions that are present and establish their amplitudes and correlation times. A comparison of experimental and calculated relaxation rates (Table V) shows that the rates calculated for a rigid rod model of DNA are about 2 times faster than the observed rates. This discrepancy would be even larger if, as is likely, the molecules are tumbling in solution more slowly than we estimate as a result of intermolecular association in the NMR samples (Genest et al., 1985). The large discrpancy between the observed and calculated rates shows that DNA does not behave as a rigid rod. Reducing the effective correlation time for the axial spinning to 6 ns to account for collective torsional motions is ineffective in reducing $R1^S$ and R_2, but reducing the end-over-end correlation time from 329 to 180 ns (effectively shortening the rod) does reduce these rates to the observed value. This shows that bending and out-of-plane motion of the bases relative to the helix must be important in the relaxation of poly(dA)·poly(dT). Because the R_1^{NS} of the imino proton is small and has a relatively large error ($R_1^{NS} = 0.4 \pm 0.4$), torsional motions alone give calculated rates that are within experimental error of the observed imino $R1^{NS}$. However, the data are better fit with the addition of high-frequency local azimuthal motions. The best fit of the imino and TH6–TH5m data can be obtained by using a model that allows fast local torsional motion of the bases (0.2–2-ns correlation time and ±20° amplitude) coupled with slower longitudinal motions of the bases along the helix axis (10–100-ns correlation time and ±25° amplitude) in addition to fast collective torsional motions of the helix (modeled by 6-ns spinning time of the helix). The data can also be fit by using a three-site jump on the surface of a cone model that allows for ±20–25° motions of the base with a single correlation time of ~3 ns. There are several important features demonstrated by these calculations.

The first point is that torsional motions alone cannot account for the observed R_1^S and R_2 values. Only when large-amplitude (20–25°) longtiudinal motions are present do we obtain good agreement with experimental results. The amplitude of the longitudinal motion axis is set by the values of $R1^S$ and R_2, but it is difficult to establish the correlation time for these motions because the end-over-end tumbling strongly affects these rates. It is apparent, however, that reasonable values for the motional amplitudes are obtained for correlation times less than ~100 ns. Since the discrepancies between the observed rates and those calculated for the rigid rod model persist even in shorter DNA (Early et al., 1980b, 1981; Clore & Gronenborn, 1984), the correlation times for the motion along the helix are evidently signifianctly faster than the upper limit of ~100 ns set by the present data. Finally, because of the large experimental error in R_1^{NS}, collective torsional motions alone give calculated rates within experimental error of the observed R_1^{NS}. However, the best fit of the observed rate is found when fast, large-amplitude local torsional motions are also included.

(*b*) *Relation to Previous Studies of Internal Motion in DNA.* The above analysis shows that poly(dA)·poly(dT) bases and sugars exhibit large-amplitude longitudinal motions (amplitude of ±25° and correlation times <70–100 ns) and fast torsional motions (amplitude of ±20° and correlation times of 0.2–2 ns) of the base and sugar groups. The sugar motion is consistent with earlier NMR measurements (Bolton & James, 1979; Early & Kearns, 1979; Hogan & Jardetzky, 1980; Levy et al., 1981, 1983; Keepers & James, 1982; Clore & Gronenborn, 1984) that show there are substantial motions in the backbone of native DNA. Previous work on poly(dA-dT)·poly(dA-dT) and the B and Z forms of poly(dG-dC)·poly(dG-dCe shows that there are large-amplitude local torsional and longitudinal motions of the bases in both of these synthetic polymers (amplitudes of ±30–35°) (Assa-Munt et al., 1984; Mirau et al., 1985). Our results for poly(dA)·poly(dT) indicate somewhat smaller amplitudes of motion (±20–25 °C), but the difference is small. Thus, there seems to be little sequence dependence of the nanosecond motions in synthetic DNA. We also point out that analysis of X-ray diffraction data for the DNA duplex $d(CGCGAATTCGCG)_2$ suggests that DNA bases in the crystalline state may undergo large-amplitude motions (±15°) and the sugar groups are even more mobile (Holbrook & Kim, 1984). If the motions are this large in a crystal, we expect even larger amplitude motion in solution.

Table VI: Interaction Geometry of the Strongest Interactions Contributing to the Observed Cross-Relaxation Rates of AH2, AH8, and TH6 Protons[a]

	B-DNA		B′-DNA		heteronomous DNA	
interaction[b]	distance (Å)/angle to helix (deg)	rel strength	distance (Å)/angle to helix	rel strength	distance (Å)/angle to helix	rel strength
AH2(5′–3′)AH2	3.65/22	1	3.72/28	1	3.76/31	1
AH2(3′–5′)AH2	3.65/22	1	3.72/28	1	3.76/31	1
AH8–AH1′	3.89/89	0.17	3.90/80	0.02	3.84/72	0.48
AH8(5′–3′)AH1′	3.53/10	1	2.61/5	1	4.46/7	1
AH8–AH2′	2.23/75	1	2.14/68	1	3.98/69	0.00
AH8(5′–3′)AH2′	3.79/42	0.04	3.73/48	0.03	1.90/19	1
AH8–AH2″	3.48/62	0.01	3.69/61	0.06	4.65/87	0.15
AH8(5′–3′)AH2″	2.09/33	1	2.32/51	1	3.55/33	1
TH6–TH1′	3.71/89	0.23	3.70/79	0.03	3.65/87	0.22
TH6(5′–3′)TH1′	3.52/11	1	2.59/6	1	3.47/10	1
TH6–TH2′	1.91/72	1	1.81/63	1	1.82/89	1
TH6(5′–3′)TH2′	3.95/45	0.01	3.91/51	0.01	4.74/47	0.00
TH6–TH2″	3.25/59	0.03	3.41/57	0.11	3.17/71	1
TH6(5′–3′)TH2″	2.19/38	1	2.40/53	1	3.16/46	0.86
AH1′–AH2″	2.43/45	1	2.29/61	1	2.39/52	1
AH1′(5′–3′)AH2″	5.81/29	0.02	5.33/34	0.02		
AH1′(3′–5′)AH2″					5.51/67	0.03
AH2–AH1′	4.47/84	1	4.51/88	1	4.55/73	0.22
AH2(5′–3′)AH1′	6.51/63	0.03	7.12/61	0.03	7.67/53	0.00
AH2(3′–5′)AH1′	5.10/41	0.36	4.44/45	0.58	3.11/53	1
AH2–TH1′(n)[c]	5.01/89	0.53	5.13/89	0.47	5.30/72	0.09
AH2–TH1′(n − 1)	7.21/61	0.03	7.59/64	0.03	8.50/55	0.00
AH2–TH1′(n + 1)	4.97/48	0.22	4.76/48	0.14	4.00/67	0.35

[a] The interaction distances and orientations relative to the helix are taken from three structures derived from X-ray data: B-DNA (Arnott, personal communication), B′DNA (Arnott & Selsing, 1974), and heteronomous DNA (Arnott et al., 1983). The angles have been adjusted to range from 0° to 90°. [b] Both *intra*nucleotide and *inter*nucleotide interactions are shown, with the direction of the *inter*nucleotide interaction as indicated. [c] See Figure 7B for diagram illustrating the notation.

(*c*) *Comparison of Structures Derived from X-ray and NMR Data.* The cross relaxation rates presented here provide information on ten interproton interactions that must now be combined with appropriate distance–geometry or other structure search program to generate a stracutre for poly(dA)·poly(dT). Because the results provide constraints on the allowed combinations of distances and orientations of the interproton vectors, these results differ from measurements on short oligonucleotides that yield only distances but not orientations. Whether this will prove advantageous remains to be seen but the number of data points per base pair obtained for poly(dA)·poly(dT) is comparable to the 13–14 interactions per base pair that were recently reported for an 11 base pair DNA duplex (Clore & Gronenborn, 1985).

Figure 8 shows plots of combinations of internuclear separation and orientation of the interaction vector relative to the helix axis for eight interproton interactions in the poly(dA)·poly(dT) helix. These allowed geometries are determined by assuming that only one interaction contributes to the observed relaxation. On the same plots are symbols representing distance and orientation relative to the helix axis for the strongest proton–proton interaction for several models, based on X-ray studies of DNA fibers (Arnott & Selsing, 1974; Arnott et al., 1983; Arnott, personal communication). Examination of Table VI shows that one interaction usually dominates all other interactions. Therefore, the geometry of the strongest interaction can be compared with the allowed geometries calculated from the relaxation rates. In those cases where a seond interaction is significant, the contribution of the second interaction to the observed relaxation can be taken into account by decreasing the displayed interaction distance (keeping the orientation relative to the helix axis constant) to show an effective interaction geometry. The largest effect occurs when there are two equal interactions contributing to the relaxation, for example, the relaxation of the AH2 by AH2 protons on neighboring bases. In this case, the effective interaction distance would be ~12% shorter than the distance shown in Figure 8.

Additional information about the helix structure is provided by the observation that the AH2 interacts more strongly with the TH1′ proton on the opposite strand than with the AH1′ on the same strand (see Figure 3B). Since the *intra*nucleotide separation between the AH2 and AH1′ is 4.5 Å, these results indicate that the cross-strand separation between the AH2 and TH1′ is less than 4.5 Å. Comparison of the various distances shown in Table VI for the AH2 interactions in the different DNA geometries shows that the strength of the AH2–TH1′ interaction eliminates the heteronomous structure since the *intra*strand interactions are predicted to be stronger than *inter*strand interactions whereas the reverse is experimentally true. The B- and B′-DNA geometries give better overall account of the *inter*strand to *intra*strand intensities, although they still do not account for the observation that the *inter*strand interactions are larger than the *intra*strand interactions.

Considering all the NMR data, it is obvious that the heteronomous model for poly(dA)·poly(dT) poorly fits the NMR results and is therefore a poor representation of the solution structure of poly(dA)·poly(dT). The AH2–H1′ interactions also eliminate a right-handed structure with parallel strands (N. Pattabiraman, personal communication). Both the B and B′ structures provide reasonable fits of the NMR data with the B form giving the best general agreement. An even better fit of the relaxation rates is achieved if the B-form structure is modified by sliding adjacent bases relative to one another and reducing the *inter*base separation to 3.24 Å (to fit the AH2–AH2 interaction) as well as altering the glycosidic bond angles and sugar puckers slightly (still retaining a syn C2′-endo configuration) to fit the AH8 and TH6 interactions with the sugar protons. In this slightly modified structure, the sugar backbones on the A and T strands are still almost identical.

Finally, we note that the AH2–H1′ interactions may prove useful in evaluating recent proposals regarding DNA–protein

interactions. Drew and Travers (1984, 1985) propose that the sequence-dependent digestion of DNA by various nucleases is due to sequence-dependent variations in the size of the minor groove. Since AH2–H1′ interactions are sensitive to the DNA conformation and minor groove width, measurements of these cross-relaxation rates may permit this proposal to be tested experimentally.

Added in Proof

In recent work (R. W. Behling, R. Rau, P. A. Kollman, and D. R. Kearns, unpublished results) we have carried out a molecular mechanics calculation on $(dA)_{10}\cdot(dT)_{10}$ in which we incorporated the structural constraints derived from the above experiments. We find that an excellent fit of the NMR data can be obtained with either a B-type structure or a somewhat modified heteronomous structure in which both the A and T sugars adopt a 2′-endo conformation. Both of these structures have comparable energies and are much lower in energy than the highly modified A-type structure that also could be made to fit the NMR data. The above results, in conjunction with the NMR studies on internal motion in the DNA, suggest that many conformational states may contribute to the time-averaged conformational state of the DNA. Molecular mechanics calculations now in progress may help to elucidate this matter.

Acknowledgments

We thank Dr. Peter Mirau for providing one poly(dA)·poly(dT) sample.

Registry No. Poly(dA)·poly(dT), 24939-09-1.

References

Abragam, A. (1978) in *The Principles of Nuclear Magnetism* (Marshall, W. C., & Wilkinson, D. H., Eds.) Chapter 8, Oxford University Press, Oxford, England.

Arnott, S., & Hukins, D. W. L. (1972) *Biochem. Biophys. Res. Commun. 47*, 1506–1509.

Arnott, S., & Selsing, E. (1974) *J. Mol. Biol. 88*, 509–521.

Arnott, S., Chandrasekaran, R., Hall, I. H., & Puigjaner, L. C. (1983) *Nucleic Acids Res 11*, 4141–4155.

Assa-Munt, N., Granot, J., Behling, R. W., & Kearns, D. R. (1984) *Biochemistry 23*, 944–955.

Behling, R. W., & Kearns, D. R. (1985a) *Biopolymers 24*, 1157–1167.

Behling, R. W., & Kearns, D. R. (1985b) in *Books of Abstracts, Fourth Conservation in Biomolecular Stereodynamics* (Sarma, R. H., Ed.) p 79, Adenine Press, Guilderland, NY.

Behling, R. W., & Kearns, D. R. (1985c) 26th Experimental NMR Conference, Asilomar, CA, April 21–25, 1985, Abstract B-6.

Benevides, J. M., & Thomas, G. J. (1985) *Biopolymers 24*, 667–682.

Bloomfield, V., Crothers, D. M., & Tinoco, I. (1974) in *The Physical Chemistry of Nucleic Acids*, Harper & Row, New York.

Bodenhausen, G., & Ernst, R. R. (1981) *J. Magn. Reson. 45*, 367–373.

Bolton, P. H., & James, T. L. (1979) *J. Phys. Chem. 83*, 3359–3366.

Broido, M. S., & Kearns, D. R. (1982) *J. Am. Chem. Soc. 104*, 5207–5216.

Challberg, S. S., & Englund, P. T. (1980) *J. Mol. Biol. 138*, 447.

Clore, G. M., & Gronenborn, A. M. (1984) *FEBS Lett. 172*, 219–225.

Clore, G. M., & Gronenborn, A. M. (1985) *EMBO J. 138*, 447–472.

Drew, H. R., & Travers, A. A. (1984) *Cell (Cambridge, Mass.) 37*, 491–502.

Drew, H. R., & Travers, A. A. (1985) *Nucleic Acids Res. 13*, 4445–4467.

Early, T. A., & Kearns, D. R. (1979) *Proc. Natl. Acad. Sci. U.S.A. 76*, 4165–4169.

Early, T. A., Feigon, J., & Kearns, D. R. (1980a) *J. Magn. Reson. 41*, 343–348.

Early, T. A., Kearns, D. R., Hillen, W., & Wells, R. D. (1980b) *Nucleic Acids Res. 8*, 5795–5812.

Early, T. A., Kearns, D. R., Hillen, W., & Wells, R. D. (1981) *Biochemistry 20*, 3764–3769.

Elias, J. G., & Eden, D. (1981) *Biopolymers 20*, 2369–2380.

Feigion, J., Leupin, W., Denny, W. A., & Kearns, D. R. (1983) *Biochemistry 22*, 5943–5951.

Genest, D., & Wahl, P. (1978) *Biochim. Biophys. Acta 52*, 502–509.

Genest, D., Mirau, P. A., & Kearns, D. R. (1985) *Nucleic Acids Res. 13*, 2603–2615.

Hagerman, P. J. (1984) *Proc. Natl. Acad. Sci. U.S.A. 81*, 4632.

Hahn, E. L. (1950) *Phys. Rev. 80*, 580–594.

Hard, T., & Kearns, D. R. (1986) *J. Phys. Chem.* (in press).

Hogan, M., LeGrange, J., & Austin, B. (1983) *Nature (London) 304*, 752–754.

Hogan, M. E., & Jardetzky, O. (1980) *Biochemistry 19*, 3460–3468.

Holbrook, S. R., & Kim, S.-H. (1984) *J. Mol. Biol. 173*, 361–388.

Hore, P. J. (1983) *J. Magn. Reson. 55*, 283–300.

Jolles, B., Laigle, A., Chinsky, L., & Turpin, P. Y. (1985) *Nucleic Acids Res. 13*, 2075–2085.

Kearns, D. R., Assa-Munt, N., Behling, R. W., Early, T. A., Feigon, J., Granot, J., Hillen, W., & Wells, R. D. (1981) in *Biomolecular Stereodynamics* (Sarma, R. H., Ed.) Vol. I, p 345–365, Adenine Press, New York.

Keepers, J. W., & James, T. L. (1982) *J. Am. Chem. Soc. 104*, 929–939.

Levy, G. C., Hilliard, P. R., Levy, L. F., & Rill, R. L. (1981) *J. Biol. Chem. 256*, 9986–9989.

Levy, G. C. Craik, D. J., Kumar, A., & Lond, R. E. (1983) *J. Biol. Chem. 256*, 9986–9989.

Lipari, G., & Szabo, A. (1982) *J. Am. Chem. Soc. 104*, 4546–4559.

Millar, D. P., Robbins, R. J., & Zewail, A. H. (1981) *J. Chem. Phys. 75*, 3649–3659.

Millar, D. P., Robbins, R. J., & Zewail, A. H. (1982) *J. Chem. Phys. 76*, 2080–2094.

Mirau, P. A., & Kearns, D. R. (1985) *Biopolymers 24*, 711–724.

Mirau, P. A., Behling, R. W., & Kearns, D. R. (1985) *Biochemistry 24*, 6200–6211.

Moore, P., & Kime, P. (1983) *Biochemistry 22*, 2615–2622.

Morris, G. A., & Freeman, R. (1978) *J. Magn. Reson. 29*, 433–462.

Pegg, D. T., Bendall, M. R., & Doddrell, D. M. (1980) *Aust. J. Chem. 33*, 1167–1173.

Sarma, M. H., Gupta, G., & Sarma, R. H. (1985) *J. Biomol. Struct. Dyn. 2*, 1057–1084.

Simpson, L. (1979) *Proc. Natl. Acad. Sci. U.S.A. 76*, 1585.

States, D. J., Haberkorn, R. A., & Ruben, D. J. (1982) J. Magn. Reson. 48, 286-292.
Thomas, G. A., & Peticolas, W. L. (1983) J. Am. Chem. Soc. 105, 993-996.
Tirado, M. M., & Garcia de la Torre, J. (1980) J. Chem. Phys. 73, 1986-1993.
Wittebort, R. J., & Szabo, A. (1978) J. Chem. Phys. 69, 1722-1736.
Woessner, D. E., Snowden, B. S., & Meyer, G. H. (1969) J. Chem. Phys. 50, 719-721.
Wu, H. M., & Crothers, D. M. (1984) Nature (London) 308, 509-513.

Observation of the Terminal Methyl Group in Fatty Acids of the Linolenic Series by a New ^{1}H NMR Pulse Sequence Providing Spectral Editing and Solvent Suppression. Application to Excised Frog Muscle and Rat Brain†

Carlos Arûs,*,‡ William M. Westler,§ Michael Bărány,‡ and John L. Markley§

Department of Biological Chemistry, College of Medicine, University of Illinois, Chicago, Illinois 60612, and Department of Biochemistry, College of Agricultural and Life Sciences, University of Wisconsin—Madison, Madison, Wisconsin 53706

Received September 16, 1985; Revised Manuscript Received February 3, 1986

ABSTRACT: A new ^{1}H NMR pulse sequence is described that combines water suppression with the selective observation of signals from coupled spin systems. The pulse sequence is easy to set up and compensates for pulse width inhomogeneity in the biological sample. Suppression of the water signal is achieved by pulses that return the water spins to their equilibrium position; spectral editing is based on the J modulation present in spin-echo spectra and its inhibition by coherent decoupling at one of the resonances of the spin system of interest. The pulse sequence, which was designed for ^{1}H NMR spectroscopy of tissue, was tested at 470 MHz on excised frog muscle and rat brain. The lactate methyl resonance of caffeine-treated frog sartorius muscle was observed selectively by irradiation at the position of its alcoholic proton. The terminal methyl signal of linolenic acid, along with other fatty acids of the linolenic series (first double bond in the ω-3 position), was observed selectively by irradiation at the position of its ω-1 methylene group. ^{1}H NMR spectra of rat brain were edited to reveal the terminal methyl of either linolenic series or all other fatty acids. The results suggest that the terminal methyl groups of fatty acids of the linolenic series (mostly docosahexaenoic acid, 22:6) have higher mobility than those of all other fatty acids.

Two major problems with ^{1}H NMR[1] spectra of cells and tissues, (i) the dynamic range barrier presented by the large water signal and (ii) the limited spectral resolution afforded by crowded spectral regions, have been dealt with successfully in recent years. Water suppression by means of a train of hard pulses (Plateau & Guêron, 1982; Hore, 1983), which obviates the need for presaturation of the water signal and its attendant cross saturation of signals from exchangeable protons, is now standard (Arûs et al., 1984a,b). The problem of overlapping resonances in tissues has been solved for coupled spin systems by using homonuclear ^{1}H double-resonance pulse sequences or "editing" sequences (Rothman et al., 1984a,b). This technique, which has been used previously to simplify spectra of proteins (Campbell & Dobson, 1975; Campbell et al., 1975) and red blood cells (Brown et al., 1977), is based on the J modulation present in spin-echo spectra; the water peak was minimized by using ^2H_2O as the solvent or by presaturating the ^1H_2O resonance. Recently, two pulse sequences have been proposed that use selective DANTE pulses (Morris & Freeman, 1978) to achieve spectral editing and water suppression (Hetherington et al., 1985; Jue et al., 1985). We explore here an alternative approach that achieves water suppression via the JR pulse sequence (Plateau & Guêron, 1982) and spectral editing via echo generation by a nonselective composite 180° pulse. We have applied this pulse sequence, which is easy to set up and provides excellent sensitivity, to studies of frog muscle and rat brain.

Most biochemical information from cells and tissues obtained by ^{1}H NMR spectroscopy has been restricted to cytosolic metabolites (Daniels et al., 1976; Brown et al., 1977; Yoshizaki et al., 1981; Agris & Campbell, 1982; Behar et al., 1983; Arûs et al., 1984a,b; Ugurbil et al., 1984; Rabenstein, 1984). However, resonances from membrane constituents also have been detected (Mountford et al., 1982; Cross et al., 1984). Recently we observed resonances from membrane phospholipids in the ^{1}H NMR spectrum of rat brain (Arûs et al., 1985). The editing pulse sequence we describe in this paper provides the means to probe further into membrane structure

† Supported by grants from the Muscular Dystrophy Association and the National Institutes of Health (RR 01077). C.A. was a recipient of a postdoctoral fellowship from the Muscular Dystrophy Association.
* Correspondence should be addressed to this author at the Department de Bioquimica, Facultat de Ciencies, Universitat Autonoma de Barcelona, Bellaterra (Barcelona), Spain.
‡ University of Illinois.
§ University of Wisconsin—Madison.

[1] Abbreviations: AQ, data acquisition; COSY, two-dimensional homonuclear correlated spectroscopy; DANTE, delays alternating with nutation for tailored excitation; EM, exponential multiplication; FID, free induction decay; FT, Fourier transform; i.d., inside diameter; JR, jump and return pulse sequence; JRE, jump and return spin-echo pulse sequence; NMR, nuclear magnetic resonance; o.d., outside diameter; rf, radio frequency; TM, trapezoidal multiplication; TT, total recycling time.

0006-2960/86/0425-3346$01.50/0